# Thermo-elastic Damping in a Capacitive Micro-beam Resonator Considering Hyperbolic Heat Conduction Model and Modified Couple Stress Theory

M. Najafi, G. Rezazadeh[*], R. Shabani

*Mechanical Engineering Department, Urmia University, Urmia, Iran*

**ABSTRACT**

In this paper, the quality factor of thermo-elastic damping in an electro-statically deflected micro-beam resonator has been investigated. The thermo-elastic coupled equations for the deflected micro-beam have been derived using variational and Hamilton principles based on modified couple stress theory and hyperbolic heat conduction model. The thermo-elastic damping has been obtained discretizing the governing equations over spatial domain and applying complex frequency approach. The effects of the applied bias DC voltage, playing simultaneously role of an external force and softening parameter, on the quality factor have been studied. The obtained results of the modified couple stress and classic theories are compared and the effects of the material internal length-scale parameter on the differences between results of two theories have been discussed. In addition, the effects of different parameters such as beam length and ambient temperature on the quality factor have been studied.

© 2012 IAU, Arak Branch. All rights reserved.

**Keywords:** Modified couple stress theory; Thermo-elastic damping; Length-scale parameter; Electrostatic force

## 1 INTRODUCTION

RECENTLY, the development of micro-electro-mechanical systems (MEMS) by engineering and scientific communities has led to tremendous achievements. Advanced tools that have emerged on the basis of modern science, the resonators [1], micro mirrors [2], micro switches [3], micro phones [4, 5] and micro pumps [6]are examples of this approach. One of the vital issues are the increasing the sensitivity of these instruments and increasing quality factor (QF). Therefore, it is important to understand the mechanisms of energy dissipation. Thermo-elastic damping (TED) in intrinsic losses is simply not manageable.

Zener [7, 8] was the first that identified the Thermo-elastic damping as a significant dissipation mechanism and he presented an analytical solution for the energy dissipation based on micro-beam properties. Then Rozshart [9] used Zener's model and experimentally showed that the TED decreases the QF of micro-beams. Landau and Lifshitz [10] introduced an exact expression for the attenuation coefficient of thermo-elastic vibration. Evoy et al. [11] and Duwel et al. [12] experimentally showed that TED is a dominant source of damping in MEMS and NEMS devices. Lifshitz and Roukes [13] took an analytical expression for the quality factor of TED in micro-beams. Guo and Rogerson [14] investigated frequency shift ratio by considering two dimensional parabolic (TDP) heat conduction model. Sun et al. [15] studied the TED with two dimensional hyperbolic (TDH) heat conduction model with one

---

[*] Corresponding author. Tel.: +98 914 145 1407; Fax: +98 441 336 8036.

*E-mail address:* g.rezazadeh@urmia.ac.ir (G.Rezazadeh).

relaxation time. Nayfeh and Younis [16] introduced an analytical expression for the QF of micro plates. Sun et al. [17-19] and Sharma et al. [20] established the equation of coupled thermo-elastic case for studying TED in circular micro plates. Rezazadeh et al. [21] studied the QF of TED in a capacitive micro-beam resonator. Vahdat et al. [22] studied the effect of axial and residual stresses on TED in capacitive micro-beam resonators.

Nowadays the capacitive actuators such as micro-beams, rectangular micro plates and circular micro plates are used widely in order to increase the QF of resonators. Recent studies show that the materials deformation behaviors have close relation to size dependence. This specific behavior appears when the characteristic size of the micro-beam is close to the internal length-scale parameter of materials [23]. Due to lack of length-scale parameter in the theories of classical mechanics, these theories can't predict and analyze the micro-beam behaviors near the internal length-scale parameter of materials [24]. Because of that the classical couple stress theory has been introduced to eliminate these difficulties [25-27]. For the classical couple stress theory, the length-scale parameter of materials was determined by experiments and it's difficult to calculate. Because of that Yang et al. [28] has developed a modified couple stress theory, in which the couple stress tensor is symmetric and only a single internal length-scale parameter get involved instead of two classical Lame's constants. Recently, an analytical expression for quality factor in an un-deflected micro-beam was introduced based on the modified couple stress theory (MCST) and classic heat conduction model by Rezazadeh et al. [29]. Capacitive micro-beam resonators usually addition to an AC voltage is subjected to a bias DC voltage which makes the micro-beam initially deflected and decreases equivalent stiffness and fundamental frequency of the micro-beam. Now we use the thermo-elasticity equation with one relaxation time TDH and electrostatic actuating. Electrostatic actuating is a fast response and simple voltage feeding actuating method. Gold and nickel micro-beam, which have a considerable length–scale parameter are considered as case studies. We consider a variable length-scale parameter for gold and nickel micro-beams as reported by Cao and Shrotriya et al. [30, 31]. For solving the dynamic equation, a step by step linearization method (SSLM) is used and Galerkin based reduced order model is provided to investigate the dynamic behaviors of micro-beams. By considering different thickness to length-scale ratios, differences between the results of the modified couple stress theory and classical theory are studied. Furthermore, the effects of the beam length and temperature change on the convergence of these two theories are studied.

## 2   MODEL DESCRIPTION

We consider an isotropic elastic prism beam as shown in Fig. 1 and both ends of the micro-beam are clamped .The length of beam shown by $L$ $(0 \le x \le L)$ and width shown by $b$ $(\frac{-b}{2} \le y \le \frac{b}{2})$ and thickness is $h$ $(\frac{-h}{2} \le z \le \frac{h}{2})$. Because of the large ratio of $L/h$, shear deformation can be neglected [32] and the beam can be considered as an Euler Bernoulli beam. The dielectric coefficient of air shown by $\varepsilon_0$, DC applied voltage shown by $V$ and $g_0$ is the initial gap between the upper and lower (ground) electrodes. $w(x,t)$ Is the beam deflection and the positive value is defined when it is downward.

As thermal boundary conditions both ends of the micro-beam are considered isothermal and the outer surfaces of the micro-beam are adiabatic. The effect of the axial stresses appears when the applied DC voltage is close to the pull-in voltage and in dynamic analysis we apply DC voltage lower than the pull-in voltage because of that we neglect the axial stress on formulation [22].
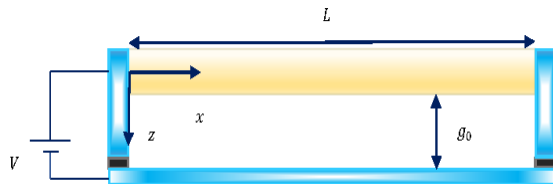


**Fig. 1**
Schematic view of the micro-beam with both ends clamped.

## 3  MATHEMATICAL EQUATION

### 3.1 Stress and strain fields

When a deformable body subjected to temperature changes the total strain field can be decomposed into the sum of thermal and mechanical components as follows [33]:

$$e_{ij} = e_{ij}^{(M)} + e_{ij}^{(T)} \tag{1}$$

Considering $\theta = T - T_0$ as the temperature variation with respect to reference temperature $T_0$, the thermal and mechanical strains for a linear, isotropic and homogenous solid can be expressed as [33]:

$$e_{ij}^{(T)} = \alpha\theta\delta_{ij}$$
$$e_{ij}^{(M)} = \frac{1+\nu}{E}\sigma_{ij} - \frac{\nu}{E}\sigma_{kk}\delta_{ij} \tag{2}$$

In this formulation, the thermal expansion coefficient $\alpha$ , the stress tensor $\sigma_{ij}$ , the kronecker delta $\delta_{ij}$ , Young's modulus $E$ and Poisson's ratio $\nu$ were indicated. The total strain field can be extracted from Eqs. (1) and (2) in term of temperature changes and stress components as following:

$$e_{ij} = \frac{1+\nu}{E}\sigma_{ij} + \left(\alpha\theta - \frac{\nu}{E}\sigma_{kk}\right)\delta_{ij} \tag{3}$$

Inverting Eq. (3), the total stress field can be expressed as:

$$\sigma_{ij} = \lambda e_{kk}\delta_{ij} + 2\mu e_{ij} - (3\lambda + 2\mu)\alpha\theta\delta_{ij} \tag{4}$$

In which $\lambda$ and $\mu$ are Lame's constant and shear modulus that can be defined in terms of Young's modulus and Poisson's ratio as follows [33]:

$$\lambda = \frac{E\upsilon}{(1+\upsilon)(1-2\upsilon)} \qquad , \qquad \mu = \frac{E}{2(1+\upsilon)} \tag{5}$$

For plane stress conditions, when the thickness (in $z$ direction) and the width (in $y$ direction) of the beam are small enough in comparison to the length (in $x$ direction) of it, the stress tensor components in $z$ and $y$ directions are considered zero [33]. ( $\sigma_{zz} = \sigma_{xz} = \sigma_{yz} = 0, \sigma_{yy} = \sigma_{xy} = \sigma_{zy} = 0$ ). Therefore ,the strain components for the plane stress condition can be simplified as following:

$$e_x = \frac{\sigma_x}{E} + \alpha\theta \qquad e_y = -\nu e_x + (1+\nu)\alpha\theta$$
$$e_z = -\nu e_x + (1+\nu)\alpha\theta \qquad e_{xy} = e_{xz} = e_{yz} = 0 \tag{6}$$

Stress tensor considering plane stress conditions has only following nonzero components in $x$ direction, which can be expressed in terms of strain and temperature changes using Eq. (6) as:

$$\sigma_x = Ee_x - E\alpha\theta \tag{7}$$

The infinitesimal components of the strain are related to the displacement gradient field by the following equation:

$$e_{ij} = \frac{1}{2}(u_{i,j} + u_{j,i}) \tag{8}$$

### 3.2 Equation of motion

The strain energy density for infinitesimal deformation is written based on the modified couple stress theory as [34]:

$$\tilde{U} = \frac{1}{2}(\sigma_{ij}e_{ij} + m_{ij}x_{ij})i \ , \quad j = 1,2,3 \tag{9}$$

where $m_{ij}$ and $x_{ij}$ is the deviatoric part of the couple stress tensor and the symmetric curvature tensor respectively. The constitutive equation relating the deviatoric part of the couple stress tensor to the symmetric curvature tensor is [34]:

$$m_{ij} = 2l^2 \mu x_{ij} \tag{10}$$

where, $l$ is the material length-scale parameter. The symmetric curvature tensor in terms of rotations gradient can be written as:

$$x_{ij} = \frac{1}{2}(\vartheta_{i,j} + \vartheta_{j,i}) \tag{11}$$

The rotation vector $\vartheta_i$ is related to the infinitesimal displacement vector as following:

$$\vartheta_i = \frac{1}{2}\varepsilon_{ijk}u_{k,j} \tag{12}$$

Applying the Euler-Bernoulli beam assumptions and denoting displacements in $x$, $y$ and $z$ directions by $u$, $v$ and $w$ respectively and choosing the origin of coordinates at the middle of the beam ($u_0 = 0$) longitudinal displacement $u = \tilde{u}(x,z,t)$ can be written in term of transversal deflection $w(x,t)$ as following:

$$u = -z\frac{\partial w}{\partial x} \tag{13}$$

By using Eqs. (6-8) and (13), the nonzero components of the strain and stress tensors in the plane stress condition can be expressed in terms of displacement field as:

$$\begin{aligned}
e_x &= \frac{\partial u}{\partial x} = -z\frac{\partial^2 w}{\partial x^2} \\
e_y &= \nu z\frac{\partial^2 w}{\partial x^2} + \alpha(1+\nu)\theta \\
e_z &= \nu z\frac{\partial^2 w}{\partial x^2} + \alpha(1+\nu)\theta \\
\sigma_x &= -Ez\frac{\partial^2 w}{\partial x^2} - E\alpha\theta
\end{aligned} \tag{14}$$

The non-zero components of $m_{ij}$ and $x_{ij}$ are extracted by substituting Eq. (13) into Eqs. (10-12) as follows [35]:

$$x_{xy} = x_{yx} = -\frac{1}{2}\frac{\partial^2 w}{\partial x^2} \quad , \quad \tilde{g}_y = -\frac{\partial w}{\partial x} \tag{15}$$

The total strain energy of the deflected beam takes the following form:

$$U = \frac{1}{2}\int_0^L \int_A \left(\sigma_x e_x + x_{xy} m_{xy} + x_{yx} m_{yx}\right) dA dx \tag{16}$$

$$U = \frac{1}{2}\int_0^L \int_{-\frac{h}{2}}^{\frac{h}{2}} \left[\left(\tilde{E}z^2 + \mu l^2\right)\left(\frac{\partial^2 w}{\partial x^2}\right)^2 + \tilde{E}\alpha_t \theta z \frac{\partial^2 w}{\partial x^2}\right] b dz dx =$$

$$= \frac{1}{2}\int_0^L \left(\tilde{E}I + \mu A l^2\right)\left(\frac{\partial^2 w}{\partial x^2}\right)^2 dx + \frac{1}{2}\int_0^L \int_{-\frac{h}{2}}^{\frac{h}{2}} b\tilde{E}\alpha_t \theta z \frac{\partial^2 w}{\partial x^2} dz dx \tag{17}$$

An electrostatic pressure that created by a DC voltage can be represented as following [32]:

$$q(w,V) = \frac{\varepsilon_0 b V^2}{2(g_0 - w(x,t))^2} \tag{18}$$

The variation of the work done by the external flexural forces per unit length $q(x,t)$ can be written as:

$$\delta W = \int_0^L q(x,t)\delta w(x,t) dx \tag{19}$$

Vibration of the beam makes a kinetic energy that can be expressed as following:

$$T = \int_0^L \frac{1}{2}\rho A\left(\frac{\partial w}{\partial t}\right)^2 dx \tag{20}$$

Now Hamilton principle can be applied to determine the equation of motion:

$$\delta\int_{t_1}^{t_2}(T - U + W) dt = 0 \tag{21}$$

By substituting Eqs. (17, 19 and 20) into Eq. (21) the equation of motion will be taken as:

$$(\tilde{E}I + \mu A l^2)\frac{\partial^4 w}{\partial x^4} + \frac{\partial^2 M_T}{\partial x^2} + \rho A\frac{\partial^2 w}{\partial t^2} = \frac{\varepsilon_0 b V^2}{2(g_0 - w(x,t))^2} \tag{22}$$

For the plane stress condition, the effective modulus $\tilde{E}$ is equal to Young's modulus $(E)$ and for a wide beam $(b \geq 5h)$ the effective modulus $\tilde{E}$ can be approximated by the plate modulus $(\frac{\tilde{E}}{1-v^2})$. In the equation of motion the moment of inertia is equal to $I = \frac{bh^3}{12}$, the cross-section area is $A = bh$ and the thermal moment is:

$$M_T = b\int_{-\frac{h}{2}}^{\frac{h}{2}} \tilde{E}\alpha_t \theta z dz \tag{23}$$

Deflection of the beam consists of two static and dynamic components. The dynamic deflection defines the vibration amplitude of the beam about its static stable equilibrium position due to the applying the DC voltage lower than the pull-in voltage.

$$w(x,t) = w_s(x) + w_d(x,t) \tag{24}$$

The dynamic deflection of micro-beam in comparison to the static deflection is too low $(w_d \langle\langle w_s)$. By using the Calculus of Variation Theory and Taylor series expansions the nonlinear electrostatic force will take the following form [32]:

$$q(w,V) = \frac{\varepsilon_0 b V^2}{2(g_0 - w_s)^2} + \frac{\varepsilon_0 b V^2}{(g_0 - w_s)^3} w_d \tag{25}$$

*3.2.1 Static equation of motion*

Substituting Eqs. (24 and 25) into Eq. (22) static deflection equation and dynamic deflection equation can be obtain. Eliminating the inertial terms the static equation of motion takes the following form:

$$(\tilde{E}I + \mu A l^2)\frac{\partial^4 w_s}{\partial x^4} - \frac{\varepsilon_0 b V^2}{2(g_0 - w_s)^2} = 0 \tag{26}$$

*3.2.2 Dynamic equation of motion*

By substituting Eqs. (24 and 25) into Eq. (22) the dynamic equation of motion takes the following form:

$$(\tilde{E}I + \mu A l^2)\frac{\partial^4 w_d}{\partial x^4} + \frac{\partial^2 M_T}{\partial x^2} + \rho A \frac{\partial^2 w_d}{\partial t^2} - \frac{\varepsilon_0 b V^2}{(g_0 - w_s)^3} w_d = 0 \tag{27}$$

*3.2.3 Generalized thermo-elasticity equation*

The coupled heat conduction equation for a thermo-elastic isotropic body with one relaxation time is given as [36]:

$$k\theta_{,ii} = \rho C_v \frac{\partial \theta}{\partial t} + \frac{E\alpha_t}{1 - 2v} T_0 \frac{\partial e_{ii}}{\partial t} + \tau_0 \rho C_v \frac{\partial^2 \theta}{\partial t^2} + \tau_0 \frac{E\alpha_t}{1 - 2v} T_0 \frac{\partial^2 e_{ii}}{\partial t^2} \tag{28}$$

Thermal conductivity shown by $k$, specific heat at constant volume shown by $C_v$ and $\tau_0$ is the relaxation time. The trace of the strain tensor for the plane stress condition can be written as:

$$e_{ii} = -(1 - 2v)\left(z \frac{\partial^2 w}{\partial x^2}\right) + 2(1 + v)\alpha_t \theta \tag{29}$$

For plane stress condition Y is defined as:

$$Y = \frac{2(1 + v)}{(1 - 2v)} \tag{30}$$

Neglecting the heat conduction in y direction and substituting Eqs. (29 and 30) into Equation of heat conduction Eq. (28) takes the following form:

$$k\left(\frac{\partial^2\theta}{\partial x^2}+\frac{\partial^2\theta}{\partial z^2}\right)=\left(\rho C_v+\mathrm{E}\alpha_t{}^2T_0\mathrm{Y}\right)\frac{\partial\theta}{\partial t}+\tau_0\left(\rho C_v+\mathrm{E}\alpha_t{}^2T_0\mathrm{Y}\right)\frac{\partial^2\theta}{\partial t^2}-ZT_0\mathrm{E}\alpha_t\frac{\partial}{\partial t}\left(\frac{\partial^2w_d}{\partial x^2}\right)-$$

$$Z\tau_0T_0\mathrm{E}\alpha_t\frac{\partial^2}{\partial t^2}\left(\frac{\partial^2w_d}{\partial x^2}\right)\tag{31}$$

In order to transform governing equations into non-dimensional forms, the Following Parameters are defined:

$$\tilde{w}_s=\frac{w_s}{g_0}\ ,\ \ \tilde{w}_d=\frac{w_d}{h}\ ,\ \ \tilde{x}=\frac{x}{L}\ ,\ \ \tilde{z}=\frac{z}{h}\ ,\ \ \tilde{\theta}=\frac{\theta}{T_0}\ ,\ \ \tilde{t}=\frac{t}{t^*}\ ,\ \ t^*=L\sqrt{\frac{\rho}{\tilde{E}}}\ ,\ \ \tilde{M}_T=\frac{M_T}{\tilde{E}bh^2}\tag{32}$$

Applying non-dimensional parameters, static equation of deflection Eq. (26) takes the following form:

$$(1+C_1)\frac{d^4\tilde{w}_s}{d\tilde{x}^4}=C_2\frac{V^2}{(1-\tilde{w}_s)^2}\tag{33}$$

and equations of dynamic deflection and heat conductions take the following forms respectively:

$$(1+C_1)\frac{\partial^4\tilde{w}_d}{\partial\tilde{x}^4}+C_3\frac{\partial^2\tilde{M}_T}{\partial\tilde{x}^2}+C_3\frac{\partial^2\tilde{w}_d}{\partial\tilde{t}^2}-C_2\frac{2\tilde{w}_dV^2}{(1-\tilde{w}_s)^3}=0\tag{34}$$

$$\frac{\partial^2\tilde{\theta}}{\partial\tilde{x}^2}+D_1\frac{\partial^2\tilde{\theta}}{\partial\tilde{z}^2}-D_2\frac{\partial\tilde{\theta}}{\partial\tilde{t}}+D_3\tilde{z}\frac{\partial}{\partial\tilde{t}}\left(\frac{\partial^2\tilde{w}_d}{\partial\tilde{x}^2}\right)-D_4\frac{\partial^2\tilde{\theta}}{\partial\tilde{t}^2}-D_5\tilde{z}\frac{\partial^2}{\partial\tilde{t}^2}\left(\frac{\partial^2\tilde{w}_d}{\partial\tilde{x}^2}\right)=0\tag{35}$$

where the appeared coefficients in these equations are:

$$C_1=\frac{12\mu l^2}{\tilde{E}h^2}\ ,\ \ C_2=\frac{6\varepsilon_0 L^4}{\tilde{E}h^3g_0{}^3}\ ,\ \ C_3=\frac{12L^2}{h^2}\ ,\ \ D_1=\frac{L^2}{h^2}\ ,\ \ D_2=\frac{L(\rho C_v+\tilde{E}\alpha_t{}^2T_0\mathrm{Y})}{k}\sqrt{\frac{\tilde{E}}{\rho}}\ ,$$

$$D_3=\frac{\alpha_t h^2\tilde{E}}{kL}\sqrt{\frac{\tilde{E}}{\rho}}\ ,\ \ D_4=\frac{\tau_0\left(\rho C_v+\tilde{E}\alpha_t{}^2T_0\mathrm{Y}\right)\tilde{E}}{k\rho}\ ,\ \ D_5=\frac{\tau_0\alpha_t\tilde{E}^2h^2}{k\rho L^2}\tag{36}$$

## 4   PROBLEM SOLUTION
### 4.1 Static deflection

Due to the nonlinearity of the equation governing the static deflection the beams, it is better to linearize it. The linearization with respect to initial gap position may cause significant errors. Therefore to decrease these errors, the SSLM method is used [32]. Based on this method, increasing the applied voltage $V_k$ to $V_k+\delta V$ leads to a small variation ($\delta w$) in the beam deflection. Using Taylor's series expansion and truncating higher order terms the nonlinear electrostatic force can be linearized about $\tilde{w}_s^k$. The variation of the deflection ($\delta w$) based on Hilbert space can be expressed in terms of basis function ($\phi_i(\tilde{x})$) as following:

$$\tilde{w}_s{}^{k+1}=\tilde{w}_s{}^k+\delta w\qquad,\qquad \delta w=\sum_{i=1}^{\infty}a_i\phi_i(\tilde{x})\tag{37}$$

where, $\phi_i(\tilde{x})$ is the basis function of the Hilbert space. To determine the unknown $a_i$ coefficients the summation series is truncated to a finite number, $N$

$$\delta w \cong \sum_{i=1}^{N} a_i \phi_i(\tilde{x}) \tag{38}$$

The equation of the static deflection at $(k+1)^{th}$ can be rewritten as following:

$$(1+C_1)(\frac{d^4 \tilde{w}_s^{k+1}}{d\tilde{x}^4}) = C_2 \left( \frac{V_{k+1}}{(1-\tilde{w}_s^{k+1})} \right)^2 \tag{39}$$

By substituting Eqs. (37 and 38) into Eq. (39), using the linear terms of the Taylor's series expansion of the electrostatic force and subtracting Eq.(33) from Eq. (39) leads to following equation:

$$(1+C_1)\sum_{i=1}^{N} a_i \phi_i^{IV}(\tilde{x}) - C_2 \frac{2V_k^2}{\left(1-\tilde{w}_s^k\right)^3} \sum_{i=1}^{N} a_i \phi_i - C_2 \frac{2V_k \delta V}{\left(1-\tilde{w}_s^k\right)^2} = R_1(\tilde{x}) \tag{40}$$

By choosing the suitable shape function, which satisfied the boundary conditions, we can solve Eq. (40) by applying Galerkin-Bobnov weighted residual method.

$$\int_0^1 \phi_j R_1(\tilde{x}) d\tilde{x} = 0 \quad j=1,\dots,N \tag{41}$$

This leads to following set of N algebraic equations.

$$\sum_{i=1}^{N} (K_{ji}^m - K_{ji}^e) a_i = F_j(\tilde{w}_s^k, V_k) \quad j=1,\dots,N \tag{42}$$

where the elements of the mechanical and electrical stiffness matrices and the forcing vector respectively are as following:

$$K_{ji}^m = (1+C_1)\int_0^1 \phi_j \phi_i^{II} d\tilde{x} \quad K_{ji}^e = 2C_2 V_k^2 \int_0^1 \frac{\phi_j \phi_i}{\left(1-\tilde{w}_s^k\right)^3} d\tilde{x} \quad F_j = 2C_2 V_k \delta V \int_0^1 \frac{\phi_j(x)}{\left(1-\tilde{w}_s^k(x)\right)^2} d\tilde{x} \tag{43}$$

By solving the obtained set of N algebraic equations, the unknown coefficients ($a_i$) are calculated at the each step and by repeating these calculations the deflection of the beam for a given applied electrostatic force is determined:

*4.2 Dynamic deflection coupled with Thermo-elastic equation*

To solve the dynamic and heat conduction equations, which are coupled, a Galerkin based reduced order model is used. This method reduces the order of equations and then the equations can be approximated in terms of linear combination of finite number of suitable shape functions with time dependent coefficient.

$$\tilde{w}_d(\tilde{x},\tilde{t}) = \sum_{r=1}^{N} q_r(\tilde{t})\phi_r(\tilde{x}) \tag{44}$$

$$\tilde{\theta}(\tilde{x}, \tilde{z}, \tilde{t}) = \sum_{i=1}^{n}\sum_{j=1}^{m} u_{ij}(\tilde{t})\varphi_i(\tilde{x})\psi_j(\tilde{z}) \tag{45}$$

where $\phi_r(\tilde{x})$ are the shape functions for the beam defection, where $\varphi_i(\tilde{x})$ and $\psi_j(\tilde{z})$ are the shape functions for the temperature variation along $x$ and $z$ directions respectively. Using Eq. (45) the non-dimensional thermal moment equation can represent as:

$$\tilde{M}_T(x) = \frac{M_T}{\tilde{E}bh^2} = \frac{T_0\beta}{\tilde{E}}\int_{\frac{-1}{2}}^{\frac{1}{2}}\tilde{\theta}z d\tilde{z} = \frac{T_0\beta}{\tilde{E}}\sum_{i=1}^{n}\sum_{j=1}^{m} u_{ij}(\tilde{t})\varphi_i(\tilde{x})\left(\int_{\frac{-1}{2}}^{\frac{1}{2}}\psi_j(\tilde{z})\tilde{z}d\tilde{z}\right) \tag{46}$$

Substituting Eqs. (44-46) into Eqs. (34) and (35) leads to following equations:

$$(1+C_1)\sum_{r=1}^{N}q_r(\tilde{t})\phi_r^{IV}(\tilde{x}) + C_3\frac{T_0\beta}{\tilde{E}}\sum_{i=1}^{n}\sum_{j=1}^{m}u_{ij}(\tilde{t})\varphi_i^{II}(\tilde{x})\left(\int_{\frac{-1}{2}}^{\frac{1}{2}}\psi_j(\tilde{z})\tilde{z}d\tilde{z}\right) +$$

$$C_3\sum_{r=1}^{N}\ddot{q}_r(\tilde{t})\phi_r(\tilde{x}) - 2C_2V^2\frac{\sum\limits_{r=1}^{N}q_r(\tilde{t})\phi_r(\tilde{x})}{(1-\tilde{w}_s)^3} = R_2 \tag{47}$$

$$\sum_{i=1}^{n}\sum_{j=1}^{m}u_{ij}(\tilde{t})\varphi_i^{II}(\tilde{x})\psi_j(\tilde{z}) + D_1\sum_{i=1}^{n}\sum_{j=1}^{m}u_{ij}(\tilde{t})\varphi_i(\tilde{x})\psi_j^{II}(\tilde{z}) - D_2\sum_{i=1}^{n}\sum_{j=1}^{m}\varphi_i(\tilde{x})\psi_j(\tilde{z})\dot{u}_{ij}(\tilde{t}) -$$

$$D_4\sum_{i=1}^{n}\sum_{j=1}^{m}\varphi_i(\tilde{x})\psi_j(\tilde{z})\ddot{u}_{ij}(\tilde{t}) + D_3\tilde{z}\sum_{r=1}^{N}\dot{q}_r(\tilde{t})\phi_r^{II}(\tilde{x}) + D_5\tilde{z}\sum_{r=1}^{N}\ddot{q}_r(\tilde{t})\phi_r^{II}(\tilde{x}) = R_3 \tag{48}$$

According to Galerkin method, following conditions should be satisfied:

$$\int_0^1\phi_f R_2\, d\tilde{x} = 0 \qquad f = 1,\ldots,N \tag{49}$$

$$\int_0^1\int_{\frac{-1}{2}}^{\frac{1}{2}}\varphi_q\psi_g R_3 d\tilde{z}\, d\tilde{x} = 0 \qquad q = 1,\ldots,n \quad , \ g = 1,\ldots,m \tag{50}$$

Application of Galerkin based reduced order model leads to $N + n\times m$ ordinary homogenous differential equations. The solution of the equations is considered in the form of $q_r = \bar{q}_r e^{i\Omega\tau}$ and $u_{ij} = \bar{u}_{ij}e^{i\Omega\tau}$, where, $\Omega$ is the complex frequency of the beam motion and heat distribution [15]. Applying the condition of achieving nontrivial solution for the obtained $N + n\times m$ algebraic equations the complex frequencies are obtained. As the value of the thermo-elastic damping is low, with a good approximation the damping ratio and quality factor can be obtained as following

$$\varsigma = \left|\frac{I(\Omega)}{R(\Omega)}\right|, \qquad Q = \frac{1}{2}\left|\frac{R(\Omega)}{I(\Omega)}\right| \tag{51}$$
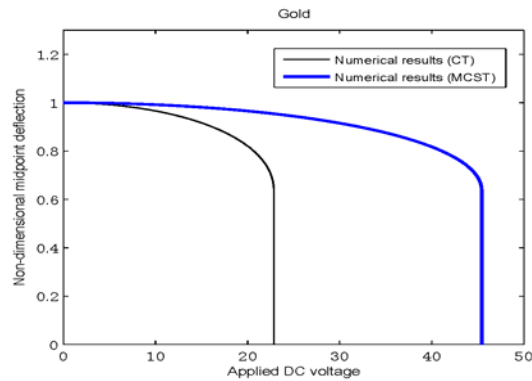
$R(\Omega)$ Is the real part of the complex frequency and $I(\Omega)$ is its imaginary part.

## 5   NUMERICAL RESULTS

We consider a wide micro beam with variable length–scale parameter and constant linear thermal expansion coefficient. The material and geometrical properties are shown in Table 1.

**Table 1**
Geometrical and material properties of the micro-beam resonator

| Parameters | Gold | Nickel |
|---|---|---|
| Length $_{(L)}$ | 200 μm | 8000 μm |
| Thickness $_{(h)}$ | 2 μm | 50 μm |
| Width $_{(b)}$ | 20 μm | 20 μm |
| Young's modulus $_{(E)}$ | 79 GPa | 210 GPa |
| Poisson's ratio $_{(v)}$ | 0.44 | 0.31 |
| Density $_{(\rho)}$ | 19320 kg/m | 8900 kg/m |
| Thermal conductivity $_{(k)}$ | 318 W/mK | 92 W/mK |
| Specific heat at constant volume $_{(C_v)}$ | 129 J/kgK | 438 J/kgK |
| Coefficient of linear thermal expansion $_{(\alpha_t)}$ | $14.2 \times 10^{-6}\,\mathrm{K}^{-1}$ | $13 \times 10^{-6}\,\mathrm{K}^{-1}$ |
| Permittivity of air $_{(\varepsilon_0)}$ | $8.8541878 \times 10^{-12}$ F/m | $8.8541878 \times 10^{-12}$ F/m |
| Ambient Temperature $_{(T_0)}$ | 300 K | 300 K |
| Initial gap $_{(g_0)}$ | 1 μm | 1 μm |
| Length-scale $_{(l)}$ | 1.05 μm for $h > 2\mu m$<br>0.73 μm for $1 < h < 2\mu m$<br>0.47 μm for $0.5 < h < 1\mu m$ | 10.8 μm for $h \le 25\mu m$<br>20 μm for $25 < h < 50\mu m$<br>28 μm for $50 \le h < 100\mu m$<br>60 μm for $h \ge 100\mu m$ |



**Fig. 2**
Non-dimensional midpoint deflection of the gold micro-beam versus the applied DC voltage.

The produced electro-static force decreases the equivalent stiffness of the micro-beam by increasing the applied DC voltage; subsequently, continuing to increase in the applied voltage causes instability of the saddle node bifurcation type [32], which is called static pull-in in the MEMS literature. In order to calculate the static deflection and pull-in voltage, the three first un-damped natural mode shapes are utilized.

It can be seen from Fig. 2 that the pull-in voltage of the golden micro-beam shifts from $22.86V$ for Classical Theory (CT) to $45.42V$ for Modified Couple Stress Theory (MCST). As a validation ,the pull-in voltage is computed by the CT using the geometrical and material properties of the previous works. The pull-in voltage of work [37] for the micro-bam with $350\mu m$ length and zero residual stress is $20.2V$ and for our code the pull-in voltage comes out $20.18V$. The accuracy of our codes is reliable and then we extend it's for MCST by our geometrical and material properties that shown in Table 1.
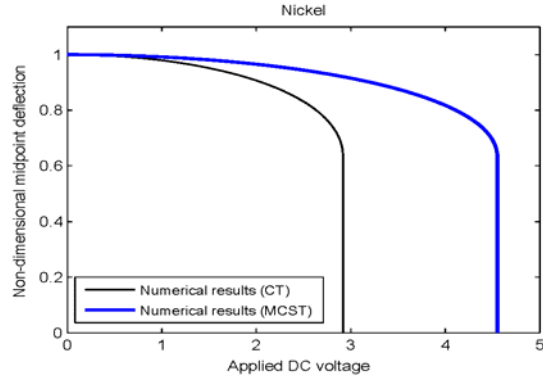
**Fig. 3**
Non-dimensional midpoint deflection of the nickel micro-beam versus the applied DC voltage.
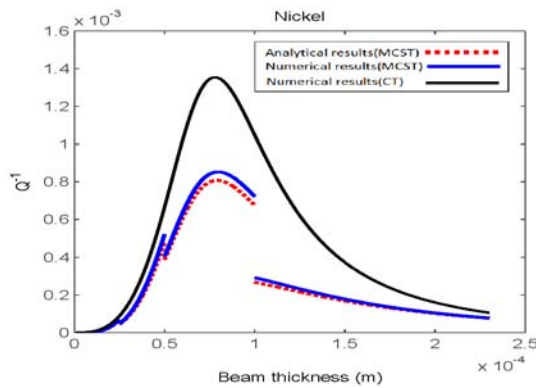


**Fig. 4**
Inverse of the quality factor versus the thickness of the nickel micro-beam .

Fig. 3 shows that the pull-in voltage of a nickel resonator, which shifts from $2.93V$ for the CT to $4.56V$ for the MCST. In order to compare the current obtained numerical results with the obtained analytical results[29], we consider the zero applied DC voltage through in the results of the Figs. 4-11 .

### 5.1 Critical thickness analysis

In a high-quality resonator, the maximum value of TED ratio occurs when the beam thickness is equal to critical thickness value [21]. For a micro-beam the characteristic or temperature relaxation time is given as [15]:

$$\tau_r = \frac{h^2}{\pi^2}\left(\frac{\rho C_v}{k}\right) \tag{52}$$

when $\tau_r \langle\langle \Omega_n^{-1}$, the micro-beam is in the isothermal condition and when $\tau_r \rangle\rangle \Omega_n^{-1}$, the micro-beam is in the adiabatic condition. The maximum TED ratio occurs when $\tau_r \Omega_n = 1$ and then we can determine the critical thickness of the micro-beam that analytically computed by the MCST [21].

$$\frac{h_{cr(MCST)}^2}{\pi^2}\left(\frac{\rho C_v}{k}\right)\times\left(\frac{4.730}{L}\right)^2\sqrt{\frac{(EI)_{eq}}{\rho A}}=1 \qquad (EI)_{eq}=EI+\mu Al^2 \tag{53}$$

We consider variable length-scale parameters for gold and nickel micro-beams [30, 31]. It can be seen from Figs. 4 and 5 that the numerical results are consistent with analytical results. When the characteristic time is equal to the inverse of vibrating frequency, thermo-elastic damping is maximized and this maximum value of TED occurs at the

specific thickness of the micro-beam that called critical thickness. As shown in Figs. 4 and 5, the differences between CT and MCST are significant at the vicinity of the critical thickness.
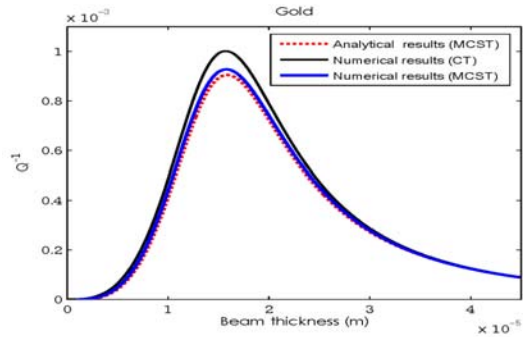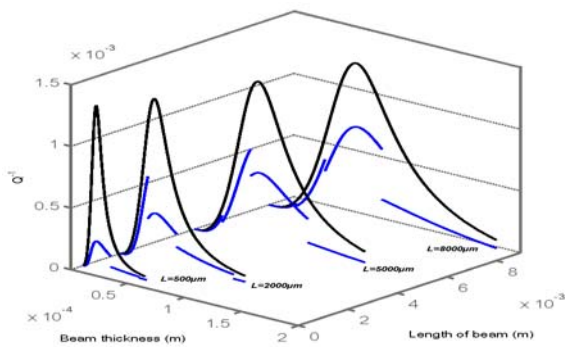


**Fig. 5**
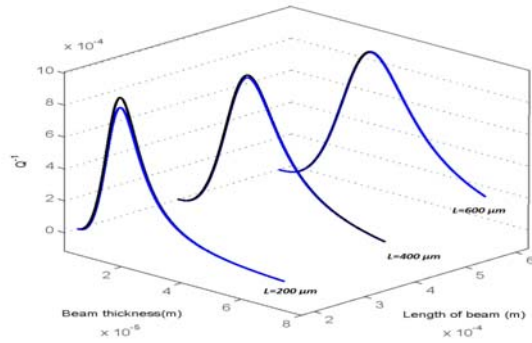Inverse of the quality factor versus the thickness of the gold micro-beam.

**Table 2**
Critical thickness value comparison

| Applied elasticity theory | Numerical results MCST | Analytical results MCST |
|---|---|---|
| | Critical thickness value (μm) | Critical thickness value (μm) |
| Gold resonator | 15.61 | 15.63 |
| Nickel resonator | 73.42 | 71.56 |

As seen in Figs. 6 and 7, the differences between the results of the modified couple stress theory and the classical theory implicitly depend on the thickness to length-scale $\left(\dfrac{h}{l}\right)$ ratios. Furthermore by increasing these ratios, the results of the two theories are converged. Evidently, by increasing the length of the micro-beam, the critical thickness occurs in higher thicknesses, but in the case of the most of the materials, the variable length-scale parameters are increasing through the increment of the thicknesses which has negative effect on increasing the thickness to length-scale $\left(\dfrac{h}{l}\right)$ ratios.



**Fig. 6**
Effect of the length and thickness of the micro-beam on the thickness to length-scale ratio of the nickel micro-beam.

**Fig. 7**
Effect of the length and thickness of the micro-beam on the thickness to length-scale ratio of the gold micro-beam .

**Table 3**
Effect of beam length to critical thickness value

| Applied elasticity theory | Numerical results MCST | Numerical results CT |
|---|---|---|
| | Critical thickness value (μm) | Critical thickness value (μm) |
| Gold (L=200μm) | 15.61 | 15.64 |
| Gold (L=400μm) | 24.1 | 24.2 |
| Gold (L=600μm) | 31.2 | 31.3 |
| Nickel(L=500μm) | 11.7 | 11.9 |
| Nickel (L=2000μm) | 30.9 | 30.5 |
| Nickel (L=5000μm) | 56.7 | 56 |
| Nickel (L=8000μm) | 73.42 | 73.40 |

*5.2 Effects of ambient temperature on thermo-elastic damping*

The effect of the temperature change on inverse of the quality factor is displayed in Figs. 8 and 9. Based on the obtained results, at higher temperatures there are much differences between the results of CT and MCST. In Figs. 8 and 9, the numerical results are coincident with analytical results.
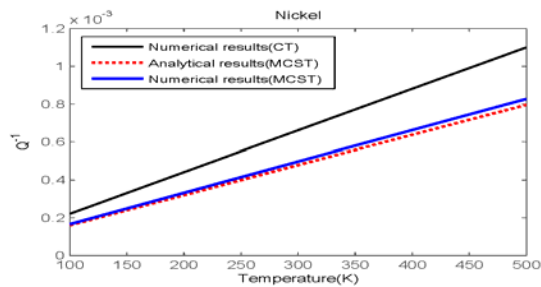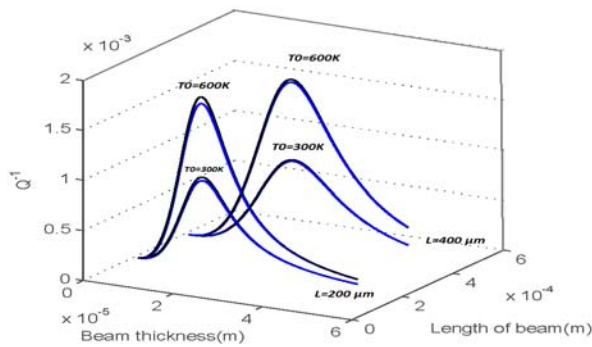


**Fig. 8**
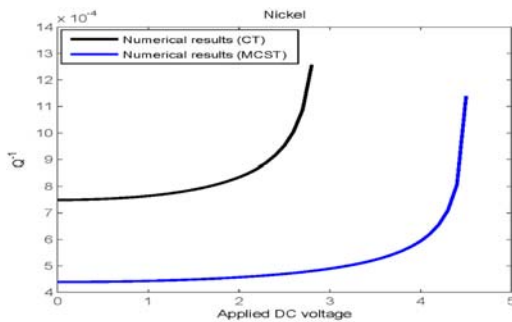Inverse of the quality factor versus temperature in the nickel micro-beam .
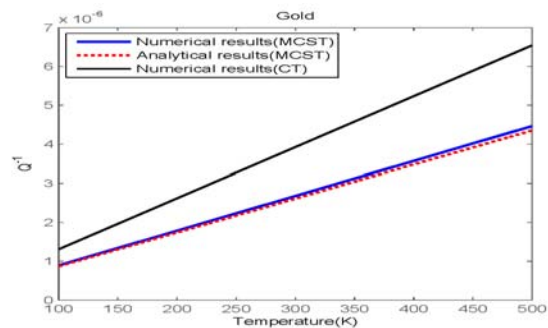


**Fig. 9**
Inverse of the quality factor versus temperature in gold micro-beam.
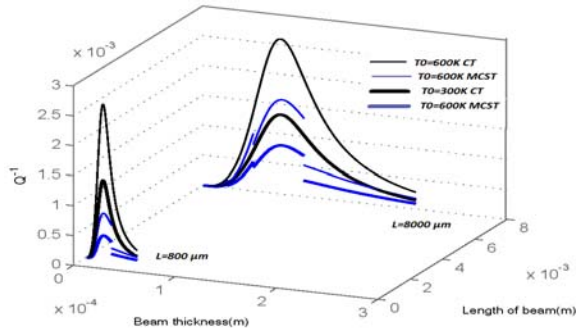
**Fig. 10**
Inverse of the quality factor versus beam thickness for different beam lengths and different temperatures in the nickel micro-beam.



**Fig. 11**
Inverse of the quality factor versus beam thickness for different beam lengths and different temperatures in the gold micro-beam.



**Fig. 12**
Effect of the applied DC voltage on the inverse of the quality factor of the nickel micro-beam.

By increasing the temperature, differences between CT and MCST are increased. The divergence of the CT and MCST at higher thickness to length-scale ratio has decreased. Figs. 10 and 11 show the inverse of the quality factor versus beam thickness for different beam lengths and different temperatures in the nickel and gold micro-beams respectively. As shown in these figures, the difference between the results of the two theories are increased by growing the temperature but by increasing the beam length this difference is decreased.

*5.3 Effects of applied voltage on thermo-elastic damping*

Figs.12 and 13 represent the behavior of inverse of the quality factor for DC voltages before the pull-in voltage. It is obvious that inverse of the quality factor increment rate, increases significantly near the pull-in voltage in comparison to the pervious DC voltages. When applied DC voltages approach static pull-in voltage the system tends to an unstable equilibrium position by undergoing to a saddle node bifurcation. Therefore, to prevent the energy losses due to the TED, applied voltage must not be close to pull-in voltage. Of course, it should be noted that based

on the MCST the stiffness of the micro-beam is greater than that on the CT and we can extend the range of the applicable DC voltages.
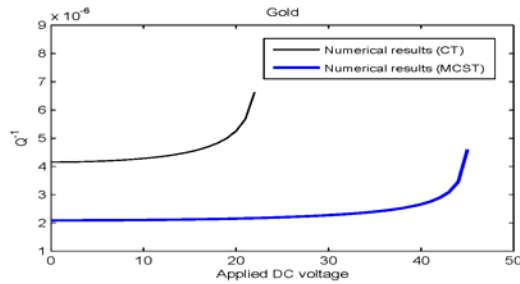


**Fig. 13**
Effect of the applied DC voltage on the inverse of the quality factor of the gold micro-beam.

## 6   CONCLUSION

In this paper, the quality factor of TED in a micro-beam resonator that electrostatically actuated was studied. The modified couple stress theory and hyperbolic heat conduction model were used and the effect of the variable length-scale parameter was shown. For some dimensions of the micro-beam, differences between the results of the CT and MCST were significant so utilizing the CT for designing leads to inaccurate performance. Differences between the results of modified couple stress theory and classical theory were depended on the thickness to length-scale ratio. By increasing this ratio, the results of the two theories were converged. Furthermore, the effects of beam length and temperature on the convergence of these two theories were shown. By increasing the temperature, differences between CT and MCST was increased and this divergence at high thickness to length-scale ratio was decreased. Moreover, was shown that the TED is increased moderately for low applied bias DC voltage and rapidly for voltages near to the pull-in threshold. The obtained results can be useful for mechanical engineers in the designing of micro resonators for MEMS applications.

## REFERENCES

[1]    Tilmans H.A., Legtenberg R., 1994, Electrostatically driven vacuum-encapsulated polysilicon resonators, Part II, Theory and performance, *Sensors and Actuators A* **45**: 67-84.
[2]    Rezazadeh G., Khatami F., Tahmasebi A., 2007, Investigation of the torsion and bending effects on static stability of electrostatic torsional micromirrors, *Microsystem Technologies* **13**: 715-722.
[3]    Ruhan M., Shen J., Wheeler C.B., 2001, latching micro electromagnetic relays, *Sensors and Actuators A* **91**: 346-350.
[4]    Chen J.Y., Hsu Y.C., Lee S.S., Mukherjee T., Fedder G.K., 2008, Modeling and simulation of a condenser microphone, *Sensors and Actuators A* **145–146**: 224-230.
[5]    Liu J., Martinn D.T., Kardirvel K., Nishida T., Cattafesta L., Sheplak M., Mann B., 2008, Nonlinear model and system identification of a capacitive dual-backplate MEMS microphone, *Journal of Sound and Vibration* **309**: 276-292.
[6]    Saif M.T.A., Alaca B.E., Sehitoglu H., 1999, Analytical modeling of electrostatic membrane actuator micro pumps, *Journal of Microelectromechanical Systems* **8**: 335–345.
[7]    Zener C., 1937, Internal friction in solids. I. Theory of internal friction in reeds, *Physical Review* **52** (3): 230-235.
[8]    Zener C., 1938, Internal friction in solids. II. General theory of thermo-elastic internal friction, *Physical Review* **53**: 90–99.
[9]    Rozshart R.V., 1990, The effect of thermo-elastic internal friction on the Q of the micromachined silicon resonators, *IEEE Solid State Sensor and Actuator Workshop*, *Hilton-Head Island*, *SC*, 13–16.
[10]   Landau L.D., Lifshitz E.M., 1959, *Theory of Elasticity*, Pergamon Press, Oxford.
[11]   Evoy S., Oikhovets A., Sekaric L., Parpia J.M., Craighead H.G., Carr D.W., 2000, Temperature-dependent internal friction  in silicon nano-electromechanical systems, *Applied Physics* **77**(15): 2397-2399.
[12]   Duwel A., Gorman J., Weinstein M., Borenstein J., Warp P., 2003, Experimental study of thermo-elastic damping in MEMS 350 gyros, *Sensors and Actuators A* **103**: 70-75.
[13]   Lifshitz R., Roukes M.L., 2000, Thermo-elastic damping in micro and nano mechanical systems, *Physical Review B* **61**: 5600-5609.
[14]   Guo F.L., Rogerson G.A., 2003, Thermo-elastic coupling effect on a micro-machined beam resonator, *Mechanics Research Communications* **30**: 513-518.

[15] Sun Y., Fang D., Soh A.K., 2006, Thermo-elastic damping in micro-beam resonators, *International Journal of Solids and Structures* **43**: 3213-3229.

[16] Nayfeh H., Younis M.I, 2004, Modeling and simulations of thermo-elastic damping in microplates, *Journal of Micromechanics Microengineering* **14**: 1711-1717.

[17] Sun Y., Saka M., 2008, Vibrations of microscale circular plates induced by ultra-fast lasers, *International Journal of Mechanical Sciences* **50**: 1365-1371.

[18] Sun Y., Tohmyoh H., 2009, Thermo-elastic damping of the axisymmetric vibration of circular plate resonators. *Journal of Sound and Vibration* **319**: 392-405.

[19] Sun Y., Saka M., 2010, Thermo-elastic damping in micro-scale circular plate resonators, *Journal of Sound and Vibration* **329**: 328-337.

[20] Sharma J.N., Sharma R., 2011, Damping in micro-scale generalized thermo-elastic circular plate resonators, *Ultrasonics* **51**(3): 352-358.

[21] Rezazadeh G., Vahdat A.S, Pesteii S.-M., Farzi B., 2009, Study of thermo-elastic damping in capacitive micro-beam resonators using hyperbolic heat conduction model, *Sensors and Transducers Journal* **108**(9): 54-72.

[22] Vahdat A.S., Rezazadeh G., 2011, Effects of axial and residual stresses on thermo-elastic damping in capacitive micro-beam resonator, *Journal of the Franklin Institute* **348**: 622-639.

[23] Shengli K., Shenjie Zh., Zhifeng N., Kai W., 2009, Static and dynamic analysis of micro-beams based on strain gradient elasticity theory, *International Journal of Engineering Science* **47**:487-498.

[24] Wang B., Zhao J., Zhou S., 2010, A microscale timoshenko beam model based on strain gradient elasticity theory, *European Journal of Mechanics-A/Solids* **29**: 591-599.

[25] Mindlin R.D., Tiersten H.F., 1962, Effects of couple-stresses in linear elasticity, *Archive for Rational Mechanics and Analysis* **11**: 415–448.

[26] Mindlin R.D., 1963, Influence of couple-stresses on stress-concentrations, *Experimental Mechanics* **3**: 1-7.

[27] Toupin R.A., 1962, Elastic materials with couple-stresses, *Archive for Rational Mechanics and Analysis* **11**(1): 385-414.

[28] Yang F., Chong A.C.M., Lam D.C.C., Tong P., 2002, Couple stress based strain gradient theory of elasticity, *International Journal of Solids and Structures* **39**: 2731-2743.

[29] Rezazadeh G., Vahdat A.S., Tayefeh-rezaei S., CetinkayaCe., 2012, Thermo-elastic damping in a micro-beam resonator using modified couple stress theory, *Acta Mechanica* **223**(6): 1137-1152.

[30] Cao Y., Nankivil D.D., Allameh S., Soboyejo W., 2007, Mechanical properties of Au films on silicon substrates, *Materials and Manufacturing processes* **22**: 187-194.

[31] Shrotriya P., Allameh S.M., Lou J., Buchheit T., Soboyejo W.O., 2003, On the measurement of the plasticity length-scale parameter in LIGA nickel foils, *Mechanics of Materials* **35**: 233-243.

[32] Rezazadeh G., Tahmasebi A., Zubstov M., 2006, Application of piezoelectric layers in electrostatic MEM actuators: controlling of pull-in voltage, *Microsystem Technologies* **12**: 1163-1170.

[33] Sad M.H, 2009, *Elasticity Theory Application and Numerics*, Elsevier Inc.

[34] Kong S., Zhou S., Nie Z., Wang K., 2008, The size-dependent natural frequency of Bernoulli–Euler micro-beams, *International Journal of Engineering Science* **46**: 427-37.

[35] Park S.K., Gao X.-L., 2006, Bernoulli–Euler beam model based on a modified couple stress theory, *Journal of Micromechanics Microengineering* **16**: 2355-2359.

[36] Khisaeva Z.F., Ostoja-starzewski M., 2006, Thermo-elastic damping in nano mechanical resonators with finite wave speeds, *Journal of Thermal stresses* **29**(3): 201-216.

[37] Osterberg P.M., Senturia S.D., 1997, A test chip for MEMS material property measurement using electrostatically actuated tests tructures, *Journal of Microelectromechanical Systems* **6**: 107-188.